Received: 22 December 2020 | Revised: 5 April 2021 | Accepted: 12 May 2021

DOI: 10.1002/2050-7038.12961

RESEARCH ARTICLE

WILEY

Brushless field-excitation method for wound-rotor synchronous machines

Syed Sabir Hussain Bukhari[1,2] | **Hamza Ahmad**[2] | **Faheem Akhtar**[1] | **Jong-Suk Ro**[2]

[1]Department of Electrical Engineering, Sukkur IBA University, Sukkur, Sindh, Pakistan

[2]School of Electrical and Electronics Engineering, Chung-Ang University, Seoul, South Korea

Correspondence
Jong-Suk Ro, School of Electrical and Electronics Engineering, Chung-Ang University, Seoul, South Korea.
Email: jongsukro@gmail.com

Funding information
Chung-Ang University Research Grants; National Research Foundation of Korea, Grant/Award Number: 2019H1D3A1A01102988

Summary

This paper proposes a simplified harmonic field-excitation scheme for the brushless operation of wound-rotor synchronous machines (WRSMs). The proposed scheme involves two inverters that are operating at different frequencies to provide an input current to the armature winding of the machine. One of these two inverters works at a frequency of 60 Hz and provides the regular three-phase fundamental current, whereas the second inverter works at 180 Hz frequency to supply the single-phase third-harmonic to the common point of the start-connected stator winding of the machine. The proposed method has the advantage that a conventional single-phase inverter can be used for generating the third-harmonic current which only needs to be operated at three times the frequency of the first inverter supplying the three-phase fundamental current. The fundamental three-phase current generates the main armature field, and the single-phase third-harmonic current produces a pulsating magnetomotive force, that induces electromotive force (EMF) in the harmonic winding of the rotor. The induced EMF is rectified to supply field current to the rotor and generates the rotor field. This field, when interacts with the main armature field, produces torque. The proposed brushless field-excitation scheme for WRSMs is implemented in JMAG-Designer version 19.1 using 2-D finite element analysis to realize its operation and analyze its performance.

KEYWORDS

brushless operation, third-harmonic field excitation, synchronous motor, wound rotor

1 | INTRODUCTION

Owing to the increasing use of rare-earth permanent magnet (PM) materials, the challenges related to the brushes and slip rings in medium- and small-scale electrical machines have been resolved by implementing brushless excitation systems using harmonics.[1-2] In Reference 3, the problem of brushed excitation has been addressed by integrating a wound rotor synchronous machine (WRSM) in an inverted configuration to feed a direct current (DC) load. In Reference 4, a hybrid excitation scheme has been designed for WRSM as an alternative to the conventional volumetric excitation part. Yet these machines are not comparable to PM machines which do not require complicated field-excitation mechanisms. Besides, the efficiency, power, torque densities, and power factor of PM machines are observed to be higher than the typical induction, and synchronous machines.[5-6] However, PM synchronous machines suffer from a few fundamental problems such as non-adjustable flux and the possibility of excitation loss. Furthermore, the cost of PM materials has increased significantly due to the increasing demand. Consequently, advancement in PM-assisted synchronous reluctance machines (SRMs) and WRSMs that either require less or no PM material has currently become a vital research trend.[7-12]

In a standard WRSM, the rotor field is energized using a supplementary field-excitation method, which generally involves exciters installed on the shaft of the machine.[13] However, these field-excitation mechanisms increase the size, cost, and weight of the machines, making them impractical for adoption in medium- and small-scale industrial applications.

To eliminate the above-mentioned inherent deficiencies associated with conventional WRSMs, several researchers have proposed brushless topologies.[14-17] These brushless topologies were developed considering third-harmonic field-excitation technology.[18]

In References 19,20, a brushless WRSM topology based on two inverters, which supplied two different magnitudes of currents to the stator winding, was proposed. In the proposed topology, the armature winding was installed using a distinct star connection distributed symmetrically in the two halves of the armature winding. This arrangement generated sub-harmonic magnetomotive force (MMF) in the airgap of the machine, which was applied to induce currents in the harmonic winding installed on the rotor. Although this topology achieves brushless operation for the WRSMs, the difference in magnitudes of the armature currents in two halves of the machine causes higher harmonics, which results in adverse effects on the output torque, efficiency, and torque ripple of the machine. Moreover, it generated a higher magnitude of unbalanced radial forces on the edges of the rotor teeth which were later addressed by implementing a machine topology with a higher number of poles for the stator winding.

In Reference 21, supplementary thyristors were employed in series with the grid and the stator winding of the machine. These thyristors/switches were operated near zero-crossing of each phase current to generate a zero-sequence third-harmonic current. The generated third-harmonic was supplied to the armature winding, which was then utilized for rotor field excitation to attain brushless operation of WRSMs. Nonetheless, this technique required complicated drive systems, which increased the overall volume and cost of the machine system. Furthermore, owing to the operation of switches near the zero-crossing and the required modification in the machine structure, it was considerably complicated to implement this brushless technique.

In Reference 12, a parallel-inverter-controlled brushless scheme that involved two inverters connected in parallel to the stator winding via thyristors was suggested. This brushless scheme is shown in Figure 1A. The inverters in this scheme worked at $a - 180^\circ$ phase-shift and were alternatingly connected and disconnected through the thyristor switches after the completion of each cycle. The composite output of the inverters generated a current waveform that contains the fundamental and third-harmonic. This third-harmonic component was utilized to excite the rotor field. Even though this technique achieved brushless operation, the usage of two three-phase inverters along with the required thyristors for the proposed operation makes it bulky and expensive.

The same composite output current shape for armature winding that was previously achieved by a parallel-inverter-controlled brushless scheme was later realized by employing an open-winding pattern-based WRSM topology in Reference 22. This brushless technique is shown in Figure 1B. The proposed scheme involves two inverters connected to both terminals of the stator winding and are operated and controlled in such a way that it resulted in the same armature current shape as achieved in the case of the parallel-inverter-controlled brushless scheme. As shown in Figure 1B, this scheme does not require any thyristor switches which make it simple and cost-effective as compared to the parallel-inverter-controlled brushless scheme without affecting the performance of the machine. However, the proposed brushless technique involves two three-phase inverters employing a sophisticated control scheme which makes it complicated to be implemented.

Considering the complications associated with the parallel-inverter-controlled and open-winding pattern-based brushless techniques, this paper proposes a simplified harmonic field-excitation scheme for the brushless operation of WRSMs. The proposed technique uses a conventional single-phase inverter with the high-frequency operation for third-harmonic current input to the common point of the star-connected stator/armature winding. The proposed method has the advantage that a conventional single-phase inverter scheme can be used for generating the third-harmonic current which only needs to be operated at three times the frequency of the first inverter supplying three-phase fundamental currents to the stator winding. Hence, it does not require any advanced and complex control design to control the stator currents. Furthermore, the proposed brushless scheme involves a single-phase inverter and does not require thyristor switches that reduce its size, weight, and cost as compared to the brushless techniques proposed in.[12,22] The three-phase fundamental current generates the main stator field, whereas the single-phase third-harmonic current induces electromotive force (EMF) in the harmonic

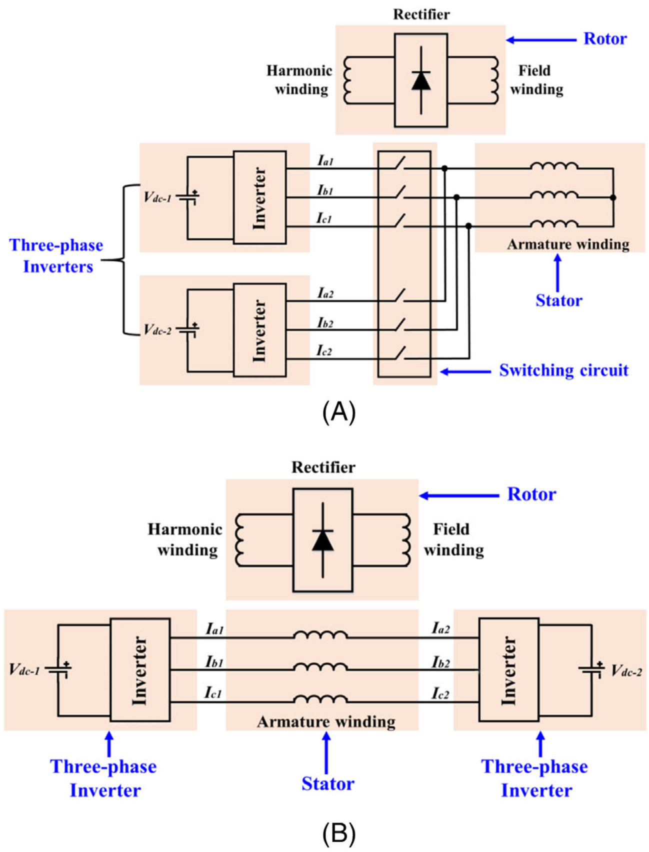

FIGURE 1 Conventional (A) parallel-inverter-controlled and (B) open-winding pattern-based brushless wound-rotor synchronous machine topologies

winding that is rectified to provide direct excitation current to the rotor field winding to achieve brushless operation of the WRSMs. The interaction of the armature and rotor fields generates torque.

2 | PROPOSED TOPOLOGY AND OPERATING PRINCIPLE

The proposed simplified brushless field-excitation scheme for WRSMs and its operating principle is discussed in the subsequent sections.

2.1 | Proposed topology

Two conventional three-phase and single-phase inverters feed currents to the stator/armature winding as illustrated in Figure 2. The three-phase inverter is operating at 60 Hz frequency and supplies a three-phase current to the stator winding. On the other hand, the single-phase inverter is connected to the common point of the star-connected armature winding and supplies a single-phase current at 180 Hz frequency. This arrangement which involves the operation of both three-phase and single-phase inverters simultaneously results in a non-sinusoidal current waveform (I_{abc}) for armature winding that consists of the fundamental and third-harmonic. The fundamental component of the armature current generates MMF in the airgap that results in the main armature field. Meanwhile, the third-harmonic component produces pulsating third-harmonic MMF in the airgap.

About the structure of the machine, the machine rotor is customized to mount the harmonic winding at the sub-pole teeth. The main role of the harmonic winding is to harvest harmonic MMF of the airgap to induce harmonic EMF in the winding. The field winding is wound around the rotor main teeth. The harmonic and field windings of the rotor are electrically connected using a full-bridge diode rectifier.

The third-harmonic MMF is applied to induce a 12-pole harmonic current in the harmonic winding of the rotor. The induced harmonic current is rectified using the diode rectifier to supply a direct rotor field-excitation current for

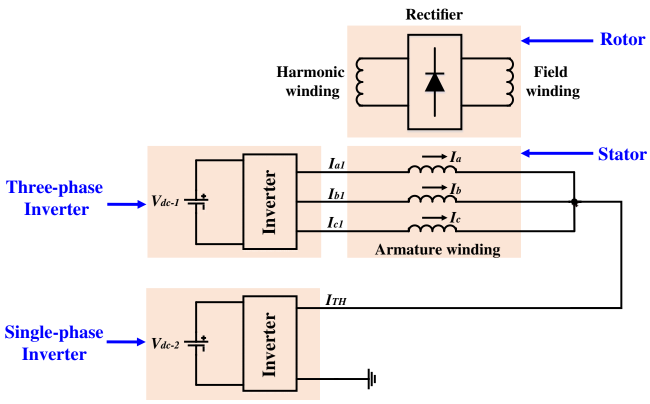

FIGURE 2 Proposed brushless wound-rotor synchronous machine topology

generating the rotor field. The proposed simplified brushless topology is validated using three machine models with different pole/slot ratio, that is, 4-pole 24-slot (4p24s), 4-pole 36-slot (4p36s), and 4-pole 42-slot (4p42s) employing double-layer stator armature winding configurations.[19]

2.2 | Working principle

The proposed simplified brushless field-excitation scheme for WRSMs employs two inverters that generate a non-sinusoidal armature current with fundamental and third-harmonic current components as illustrated in Figure 2. The inverters used for generating three-phase sinusoidal currents of 60 Hz and single-phase sinusoidal current of 180 Hz have a very traditional configuration. The output current waveforms of the three-phase inverter (I_{abc1}) and single-phase inverter (I_{TH}) are illustrated in Figure 3A,B, respectively. Figure 3C presents the composite armature winding current (I_{abc}), obtained through the proposed topology. To examine the harmonics of the input stator/armature current, a fast Fourier transform (FFT) plot is generated for phase A of the armature current, as shown in Figure 3D. The FFT plot indicates two components of the armature current, that is, fundamental, and third-harmonic currents with a magnitude of 1.3 and 1.25 A, respectively. The sum of the three-phase input armature currents that result in a third-harmonic current waveform is illustrated in Figure 3E. It reveals that the sum of third-harmonic currents in three phases displaced at 120° electrical degrees apart cannot be equal to zero, unlike the fundamental three-phase armature winding currents. Also, it can be seen that the flux generated due to this current must be pulsating instead of rotating in space.

The input armature current, which consists of the fundamental and third-harmonic currents, is expressed in (1):

$$\begin{aligned} i_a &= I_1(\sin \omega t + k \sin 3\omega t) \\ i_b &= I_1\left[\sin\left(\omega t - \frac{2\pi}{3}\right) + k \sin 3\left(\omega t - \frac{2\pi}{3}\right)\right] \\ i_c &= I_1\left[\sin\left(\omega t + \frac{2\pi}{3}\right) + k \sin 3\left(\omega t + \frac{2\pi}{3}\right)\right] \end{aligned} \tag{1}$$

where i_a, i_b, and i_c are the three-phase currents; I_1 is the peak amplitude of the fundamental; and k is the third-harmonic peak amplitude ratio.

The resultant MMF generated from each phase of the armature currents is given by

$$\begin{aligned} F_a &= i_a N_\phi[\sin \theta_e] \\ F_b &= i_b N_\phi\left[\sin\left(\theta_e - \frac{2\pi}{3}\right)\right] \\ F_c &= i_c N_\phi\left[\sin\left(\theta_e + \frac{2\pi}{3}\right)\right] \end{aligned} \tag{2}$$

where

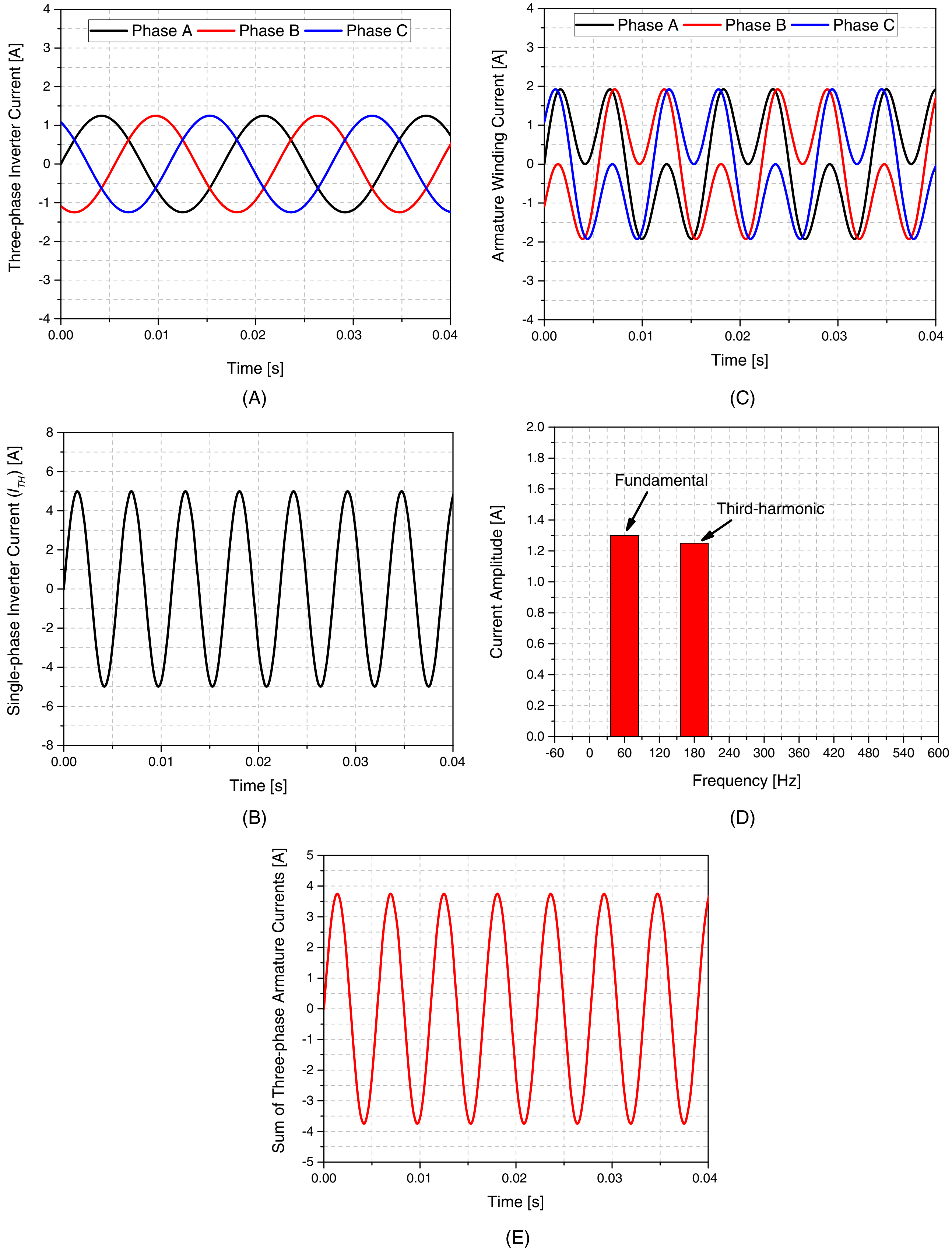

FIGURE 3 A, Three-phase inverter output current (I_{abc1}); B, single-phase inverter output current (I_{TH}); C, armature winding currents (I_{abc}); D, fast Fourier transform plot of phase A of the armature current; and E, sum of the three-phase armature currents for the proposed brushless wound-rotor synchronous machine topology

$$N_\phi = \frac{4}{\pi}\frac{N}{2}$$

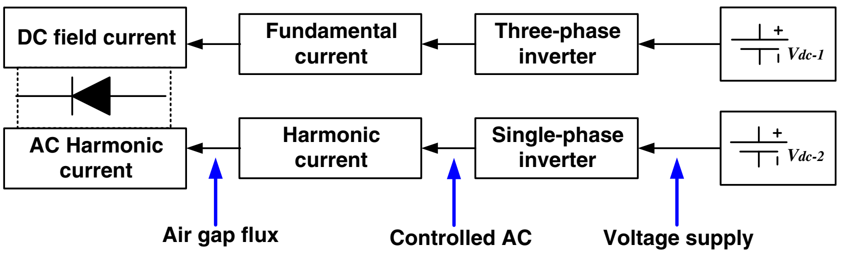

FIGURE 4 Working principle of the proposed brushless wound-rotor synchronous machine topology

TABLE 1 Specifications of the investigated machine models

Attribute	4p24s model	4p36s model	4p42s model
Rated power (in kW)	1	1	1
Stator outer/inner diameter (in mm)	177/100	177/100	177/100
Air gap (in mm)	0.5	0.5	0.5
Rotor outer diameter (in mm)	99	99	99
Machine poles/Stator slots	4/24	4/36	4/42
Stator winding number of turns	20	20	20
Harmonic/field winding number of turns	9/150	9/150	9/150
Stack length (in mm)	80	80	80

TABLE 2 FEA parameters for the investigated machine models

Attribute	4p24s model	4p36s model	4p42s model
Rotational speed	1800	1800	1800
Boundary conditions	1.5*177 mm	1.5*177 mm	1.5*177 mm
Number of divisions	21 600	21 600	21 600
Time interval/1 Step	92.5 μs	92.5 μs	92.5 μs
Number of steps	21 601	21 601	21 601
Number of elements	18 797	18 797	18 797
Number of nodes	14 449	14 449	14 449

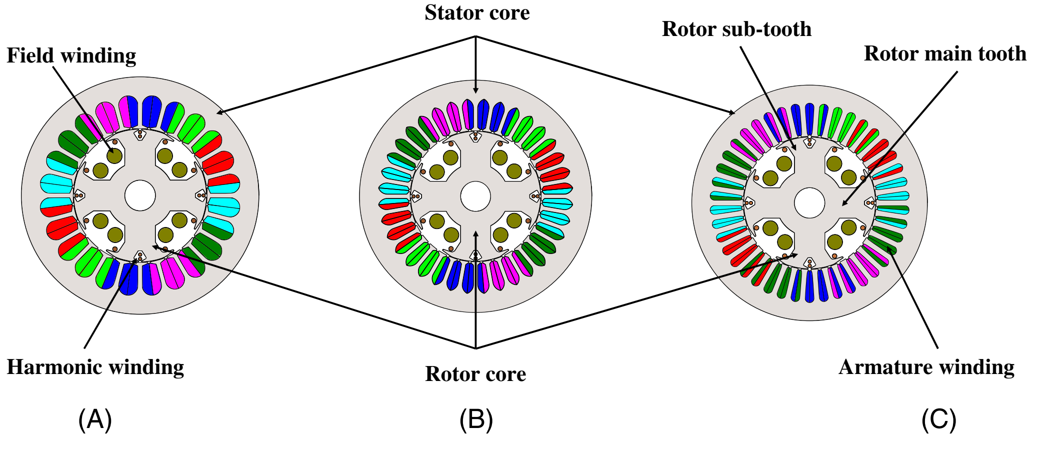

FIGURE 5 Machine models (A) 4p24s, (B) 4p36s, and (C) 4p42s

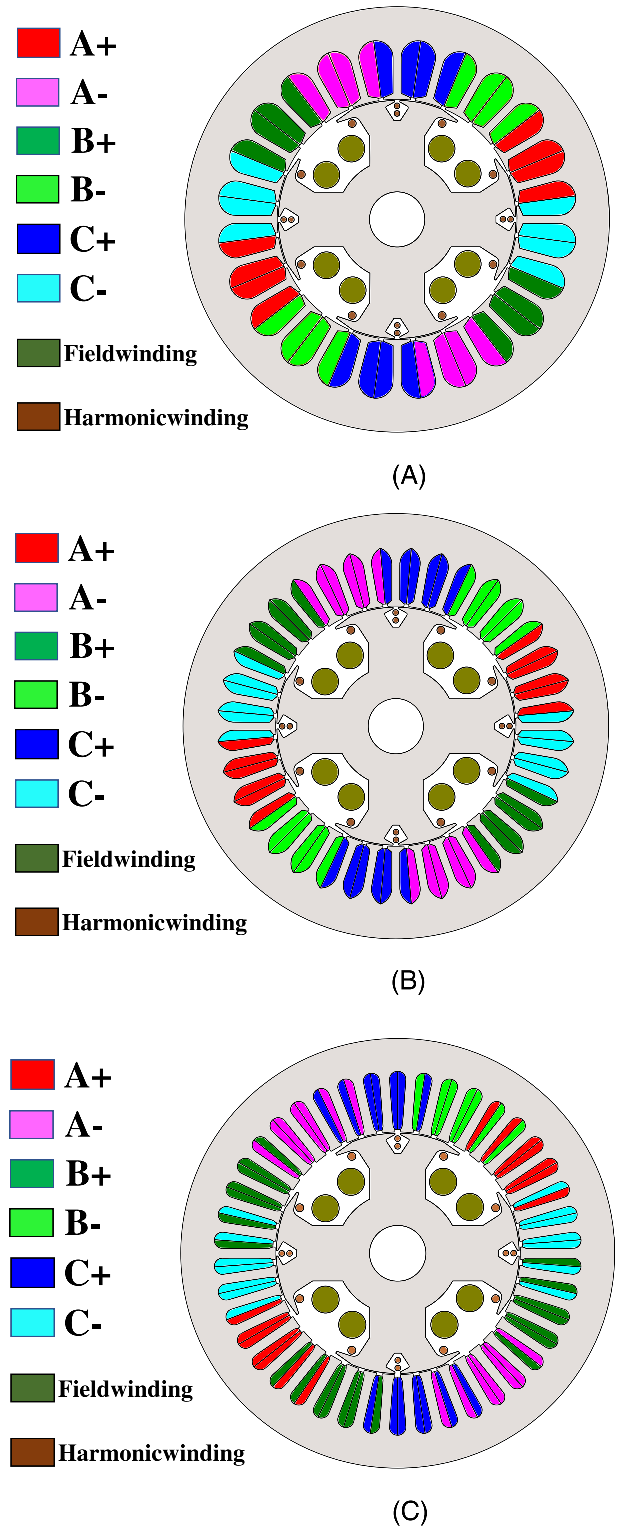

FIGURE 6 Machine winding pattern for (A) 4p24s, (B) 4p36s, and (C) 4p42s models

Here, N is the winding turns per phase; and $\theta_e = \omega t + \theta_o$, where θ_e is the electrical angle, and θ_o is the initial rotor position.

The machine airgap MMF caused by the stator currents is:

$$F_{abc}(\theta_e, i_{abc}) = F_a + F_b + F_c$$
$$= \frac{3}{2} I_1 N_\phi \cos(\omega t - \theta_e) + I_3 N_\phi \cos 3(\omega t + \theta_e) \quad (3)$$

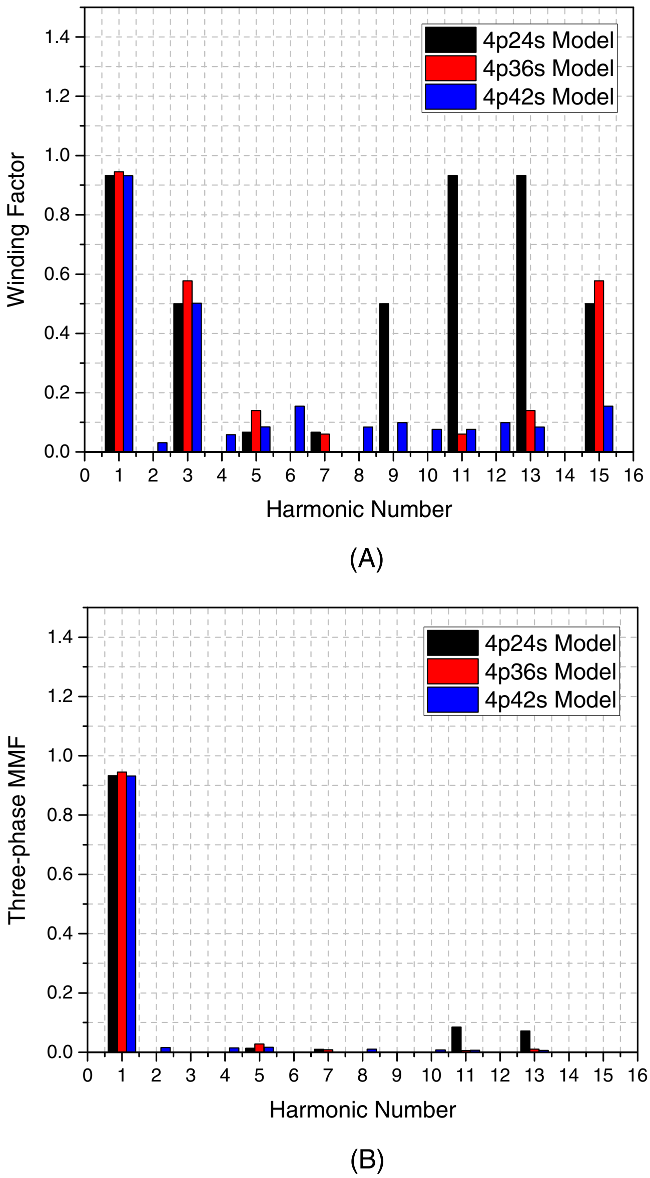

FIGURE 7 (A) Winding factors and (B) three-phase magnetomotive force for different harmonic numbers generated for the employed stator windings

TABLE 3 Winding parameters for the investigated machine models

Attribute	4p24s model	4p36s model	4p42s model
Number of poles/slots	4/24	4/36	4/42
Number of layers	2	2	2
Coil span	5 slots	8 slots	9 slots
Pole pitch	6 slots	9 slots	10.5 slots
Winding factor and fundamental MMF	0.933	0.945	0.932

Abbreviation: MMF, magnetomotive force.

where F_{abc} is the total MMF generated by all three phases of the input armature currents.

The first term in Equation (3) represents the fundamental current, whereas the second term of the equation indicates the third-harmonic current, which is then induced in the harmonic winding of the rotor, as expressed by the following:

$$\psi_h = N_h N_\varphi P_g \left(\frac{3}{2} I_1 \cos(\omega t - \theta_e) + k I_3 \cos(3\omega t + 3\theta_e) \right) \tag{4}$$

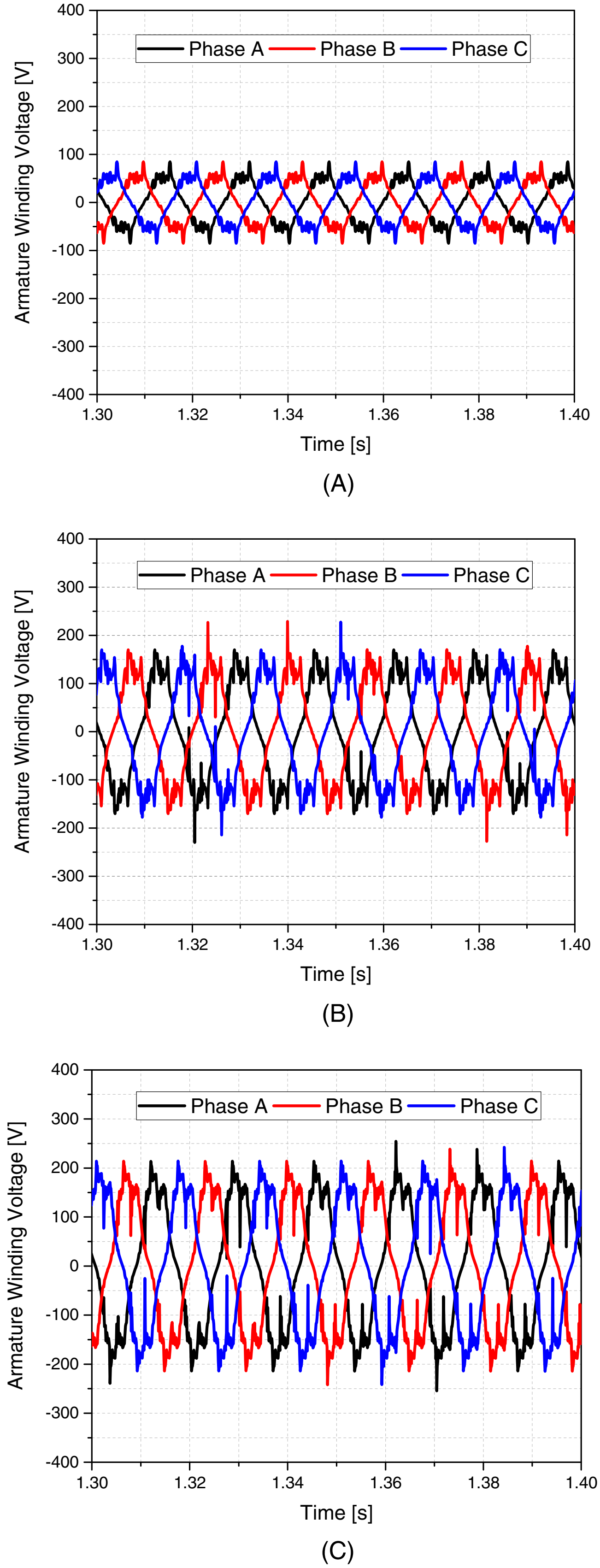

FIGURE 8 Armature winding voltages for (A) 4p24s, (B) 4p36s, and (C) 4p42s machine models

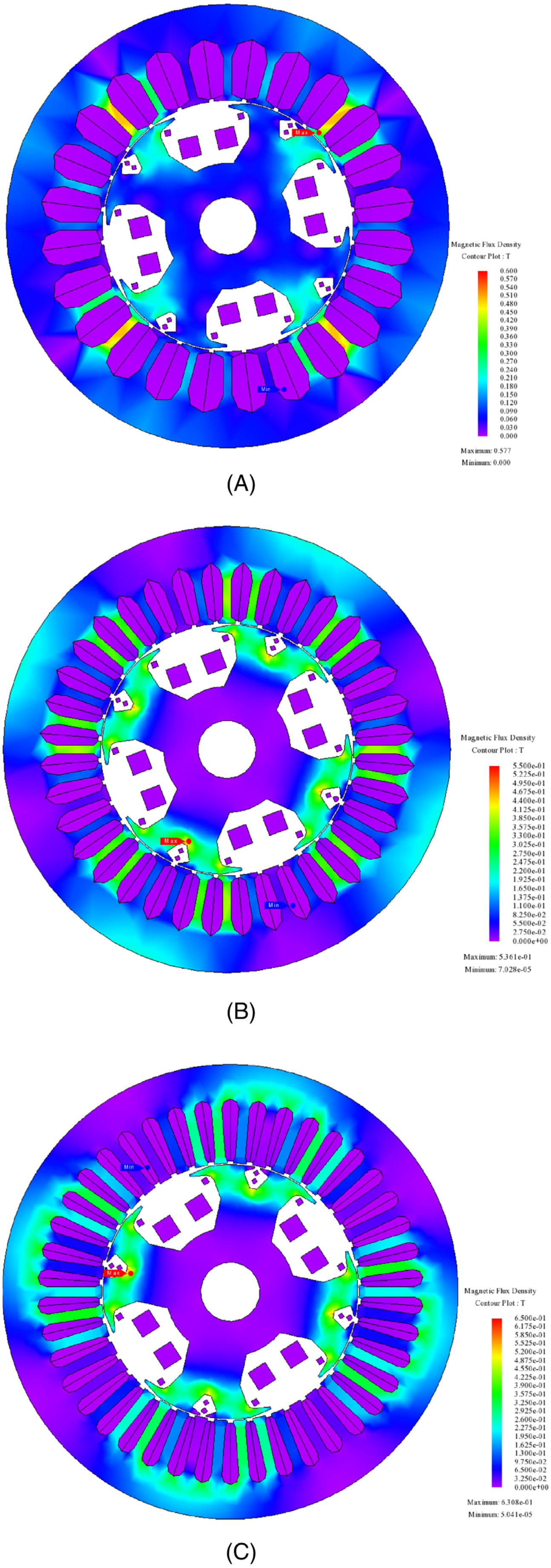

FIGURE 9 Magnetic field density distribution plots of (A) 4p24s, (B) 4p36s, and (C) 4p42s machine models under the saturation limit of 0.65T

FIGURE 10 Flux linkages for (A) 4p24s, (B) 4p36s, and (C) 4p42s machine models

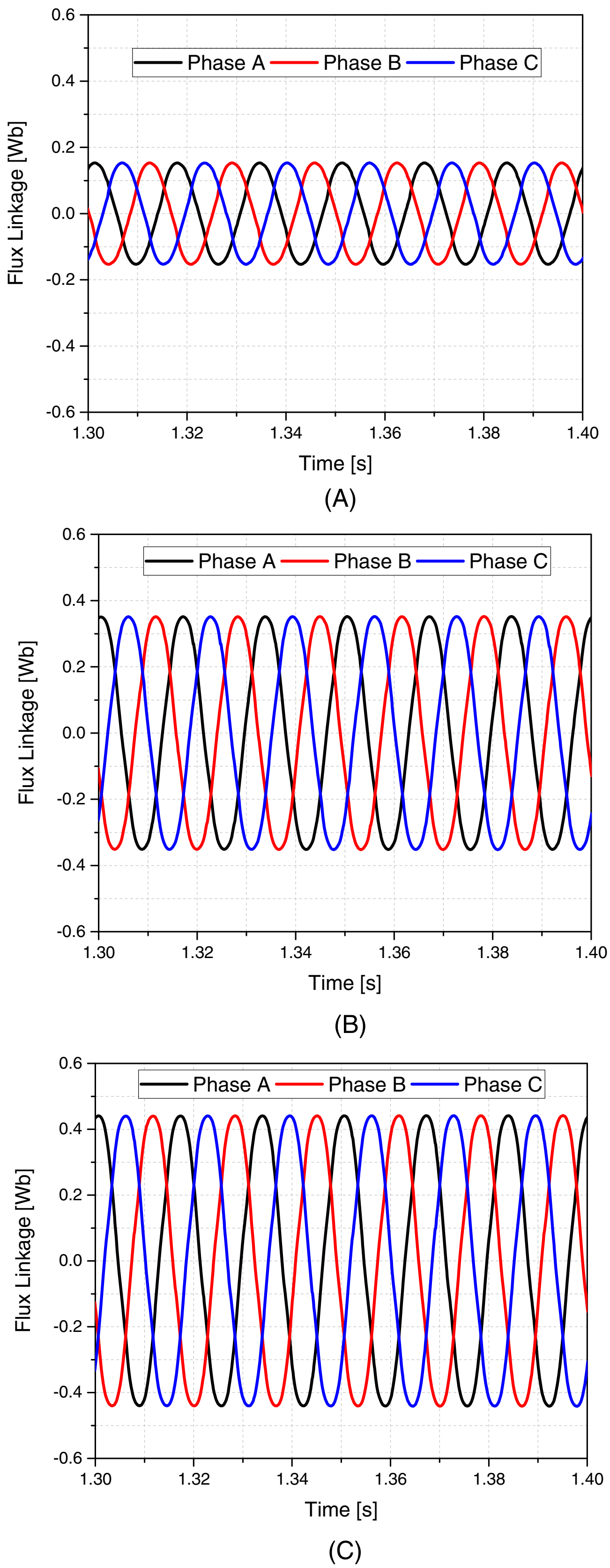

where N_h is the number of turns of the harmonic winding, and P_g is the airgap permeance.

The induced EMF due to the third-harmonic MMF component in the harmonic winding of the rotor is given by[21,23]:

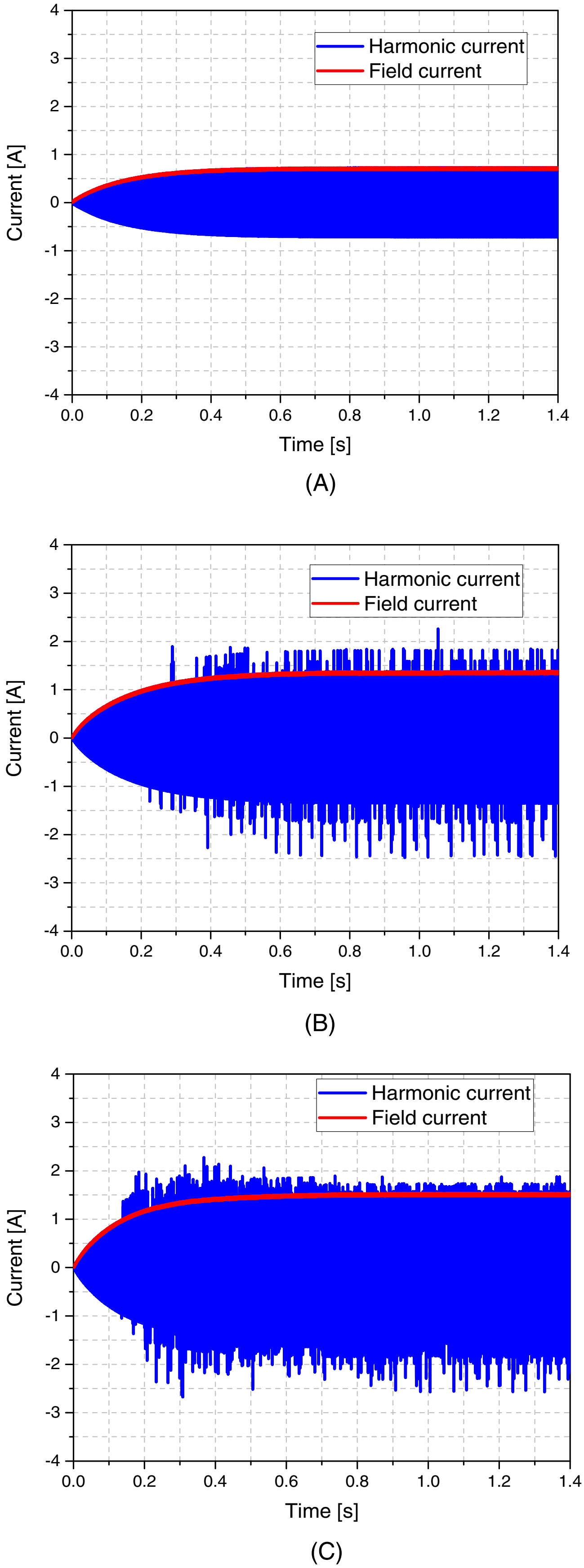

FIGURE 11 Induced harmonic and field currents for (A) 4p24s, (B) 4p36s, and (C) 4p42s machine models

FIGURE 12 Induced harmonic and field voltages for (A) 4p24s, (B) 4p36s, and (C) 4p42s machine models

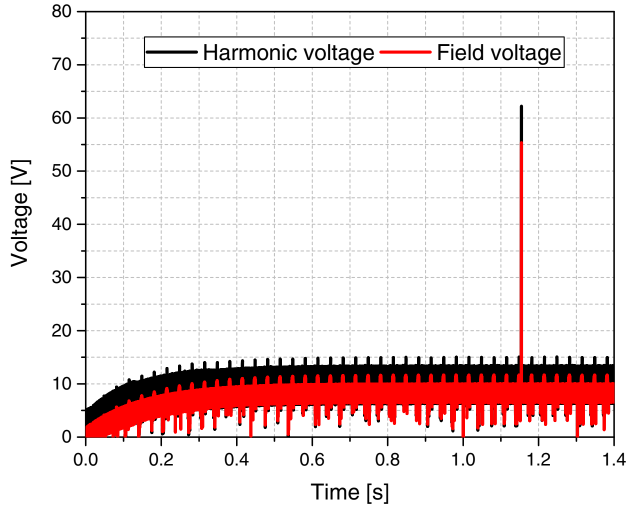

(A)

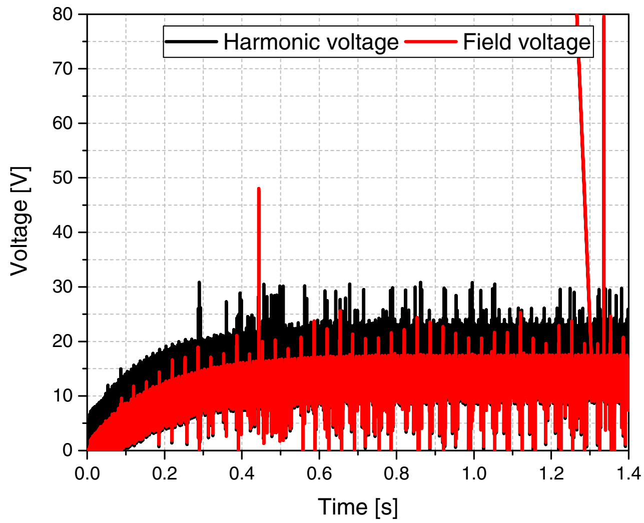

(B)

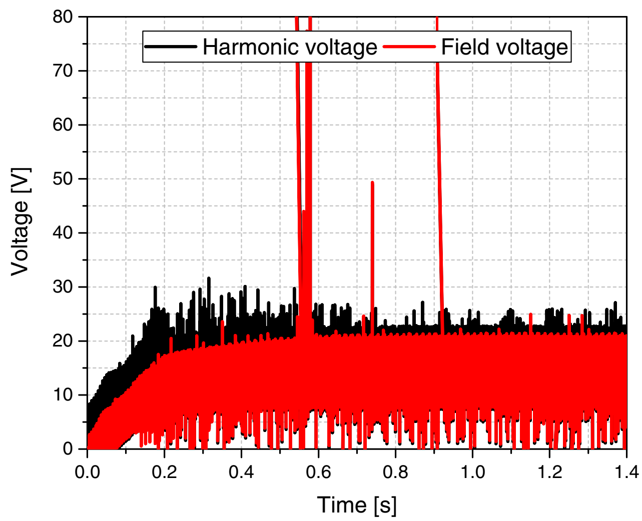

(C)

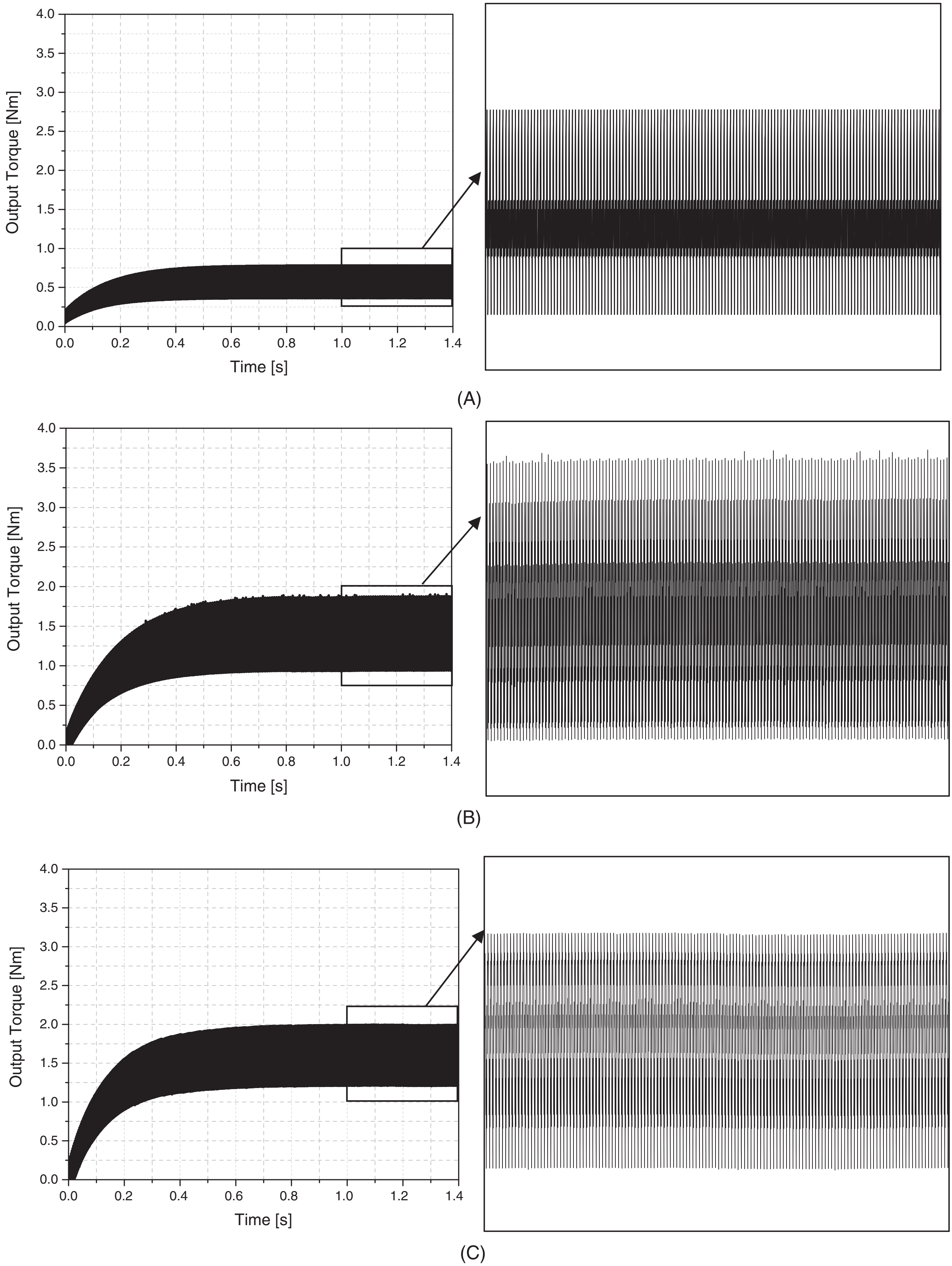

FIGURE 13 Output torque of (A) 4p24s, (B) 4p36s, and (C) 4p42s machine models

FIGURE 14 Fast Fourier transform plots of torque profiles for (A) 4p24s, (B) 4p36s, and (C) 4p42s machine models under steady-state condition

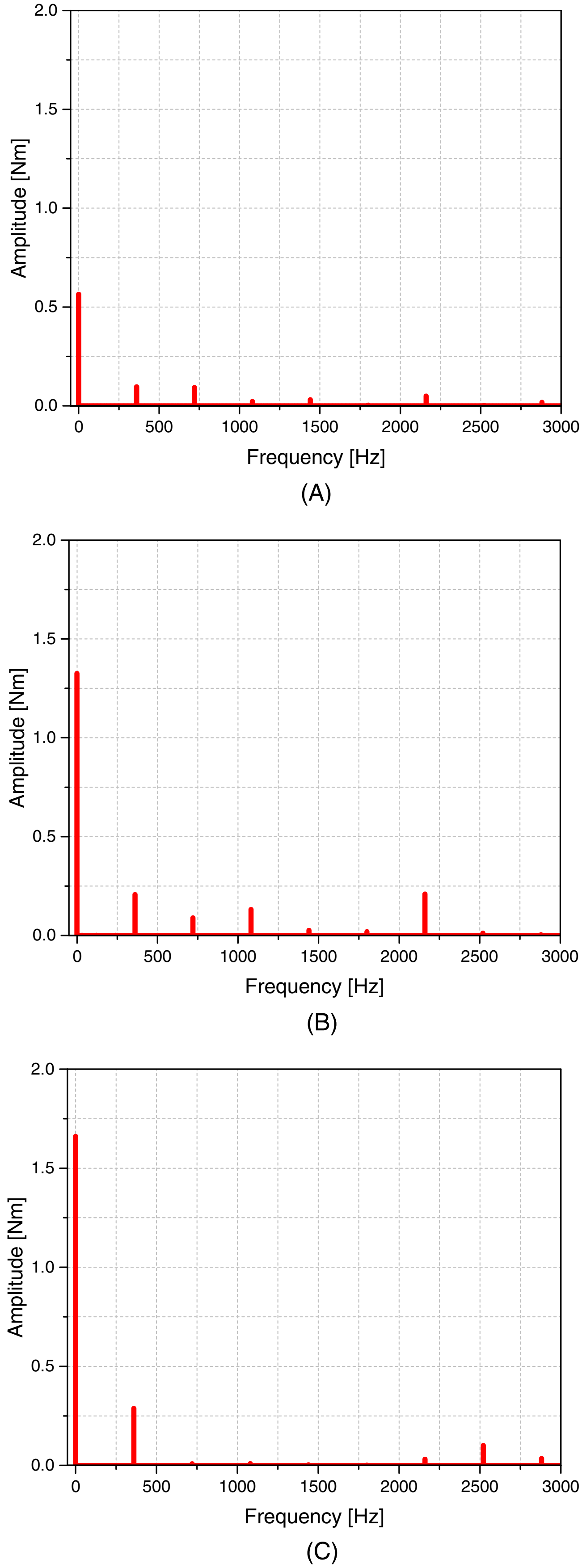

TABLE 4 Performance comparison

Attribute	4p24s model	4p36s model	4p42s model
Average output torque (in Nm)	0.564	1.326	1.661
Maximum output torque (in Nm)	0.782	1.885	1.995
Torque ripple (%)	74.18	71.22	47.06
Average radial force (in N)	0.036	0.278	0.149

$$EMF_h = 6\frac{d\psi_h}{dt} = 18N_hN_\phi P_gI_3\omega\sin3(2\omega t+\theta_0) \quad (5)$$

The induced EMF in the harmonic winding is rectified using the full-bridge rectifier to generate a DC for rotor field excitation, which then interacts with the main armature field to produce torque. The working principle of the proposed simplified brushless field-excitation scheme for WRSMs is shown in Figure 4.

3 | ELECTROMAGNETIC ANALYSIS

To validate the proposed simplified brushless field-excitation scheme for WRSMs, FEM is employed to perform finite element analysis (FEA) using JMAG-Designer version 19.1 for three machine models having different pole/slot ratios, that is, 4p24s, 4p36s, and 4p42s. The parameters of these machine models are listed in Table 1 and the conditions for carrying out FEA for the investigated machine models are presented in Table 2. Figure 5 shows the investigated machine models, and their stator and rotor winding configurations are illustrated in Figure 6. The winding factors and three-phase MMF for the different harmonic numbers generated for the employed stator windings for 4p24s, 4p36s, and 4p42s machine models are shown in Figure 7A,B, respectively. From these figures, it can be seen that the winding factor and the three-phase MMF for the fundamental harmonic of the employed stator winding for 4p24s, 4p36s, and 4p42s machine models are 0.933, 0.945, and 0.932. The detailed parameters of the stator windings for the investigated machine models are shown in Table 3.

A three-phase inverter is connected with the stator winding of the investigated machine models and supplies I_{abc1} of magnitude 1.3 A (peak) at the frequency of 60 Hz. On the other hand, a single-phase inverter is connected to the common point of the star-connected stator winding and supplies I_{TH} of magnitude 5 A (peak) at 180 Hz frequency. The net stator winding current attains a peak of 2 A with a shape that contains fundamental as well as third-harmonic current components. The fundamental component generates the main stator field, which is rotating in nature, while the third-harmonic component generates the harmonic field which is pulsating in nature. The investigated machine models are operated at a constant speed of 1800 rpm and the simulations are performed for 1.4 seconds. The armature voltages of the investigated machine models when they are supplied with a three-phase fundamental current of 1.3 A (peak) and a single-phase third-harmonic current of 5 A (peak) through an arrangement discussed above are shown in Figure 8. The magnetic field density distribution plots of 4p24s, 4p36s, and 4p42s machine models are shown in Figure 9. These plots indicate that the operation of machine models employing the proposed simplified harmonic field-excitation scheme is under the saturation level of 0.65T. The flux linkages of the investigated machine models are shown in Figure 10. The magnitude of flux linkages for the 4p24s machine model under the steady-state operation is 0.153 Wb (peak), whereas the peak values of the flux linkages for 4p36s and 4p42s machine models are 0.351 and 0.441 Wb, respectively.

The pulsating magnetic field caused by the harmonic current of the stator winding induces the EMF in the harmonic winding of the specially designed rotor which is later rectified using the full-bridge diode rectifier to supply the direct field-excitation current to the field winding of the rotor. Figure 11 illustrates the behavior of the induced harmonic and rectified field currents of the investigated machine models. This figure shows that the average magnitude of the rectified field current in the case of the 4p24s machine model is around 0.644 A; however, the magnitude of the same current for 4p36s and 4p42s machine models is 1.246 and 1.378 A, respectively. The behavior of the induced harmonic and rectified field voltages is illustrated in Figure 12 which shows that the average rectified field voltage for the 4p24s machine model is around 8.136 V, whereas the magnitude of rectified field voltages for 4p36s, and 4p42s machine models are 13.598 and 14.119 V, respectively.

FIGURE 15 Radial force plot for (A) 4p24s, (B) 4p36s, and (C) 4p42s machine models

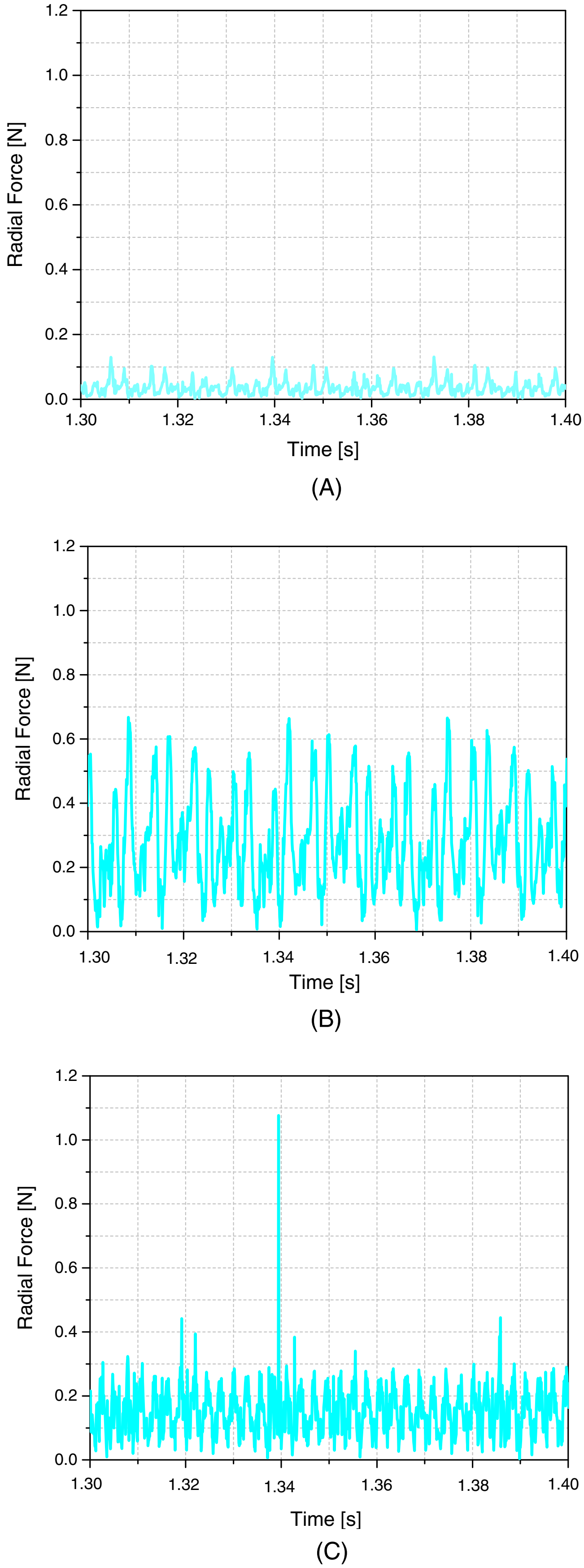

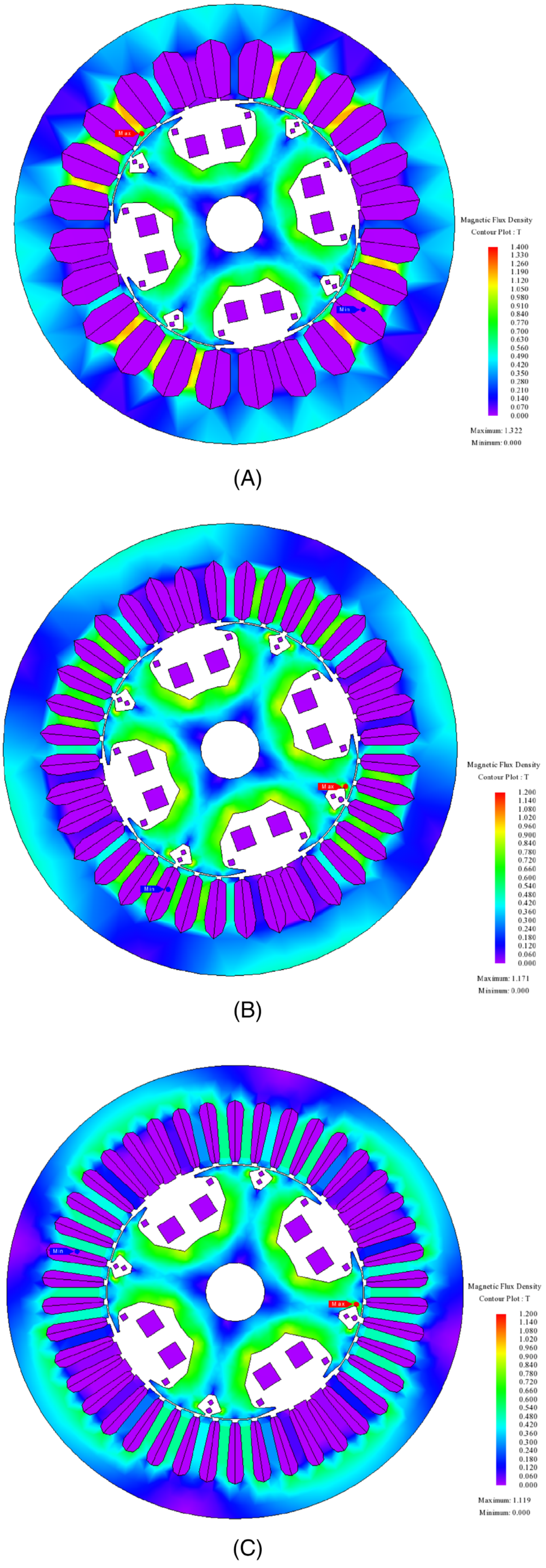

FIGURE 16 Magnetic field density distribution plots under the no-load condition for (A) 4p24s, (B) 4p36s, and (C) 4p42s machine models

FIGURE 17 Induced back-electromotive force under the no-load condition for (A) 4p24s, (B) 4p36s, and (C) 4p42s machine models

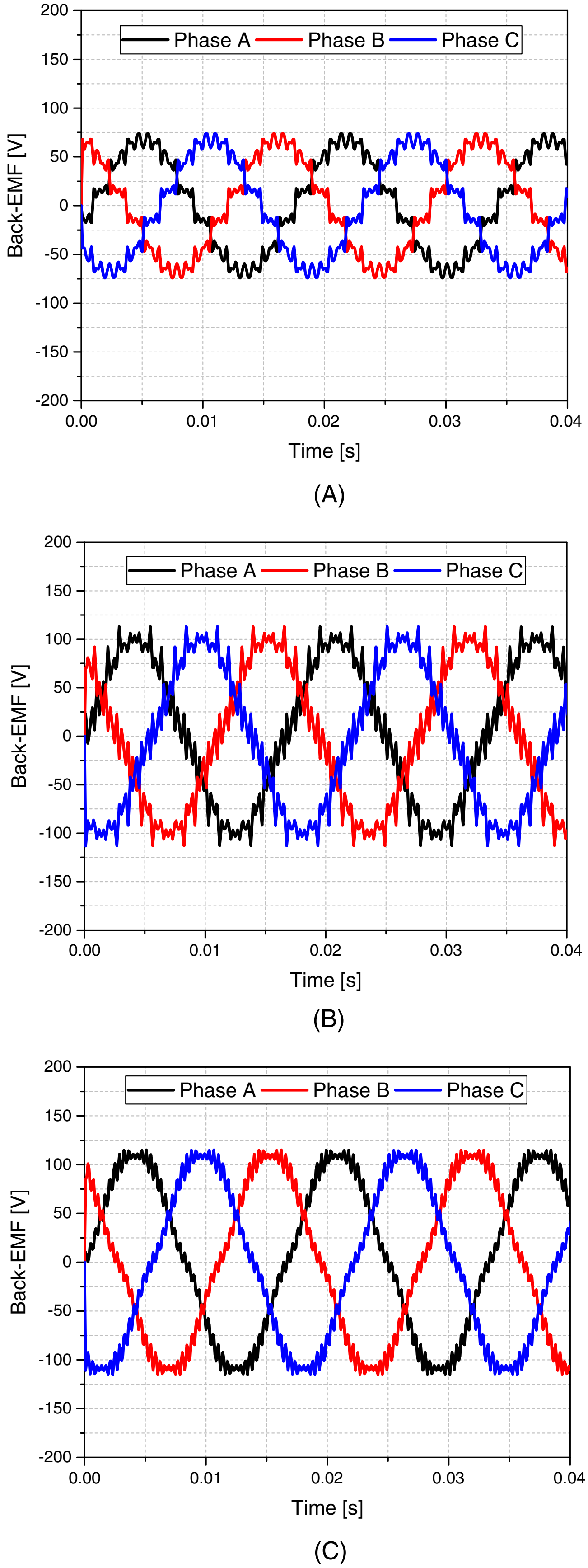

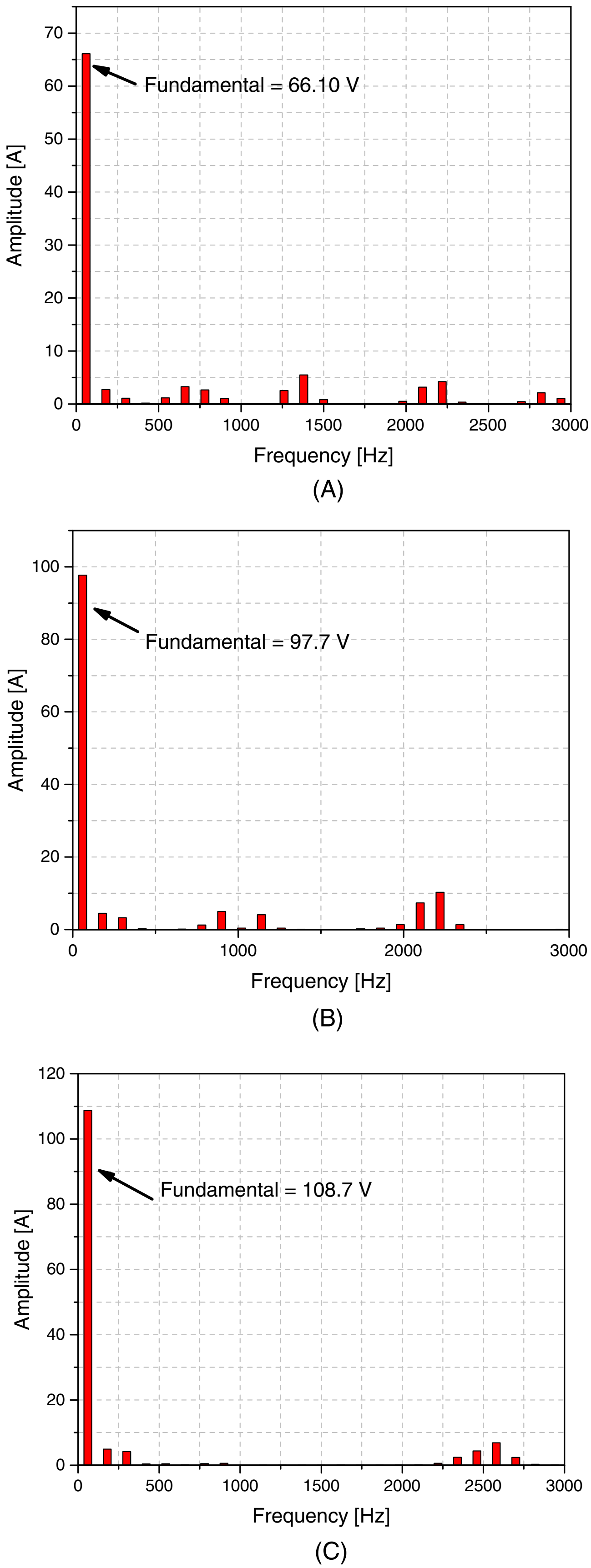

FIGURE 18 Harmonic contents of the induced back-electromotive force under the no-load condition for (A) 4p24s, (B) 4p36s, and (C) 4p42s machine models

The rectified field current generates the main rotor field, which interacts with the main armature field to generate torque. The magnitude of the average torque for 4p24s and 4p36s machine models is around 0.564 and 1.326 Nm, respectively; however, the same magnitude for the 4p42s machine model is around 1.661 Nm. The output torque of the investigated machine models is shown in Figure 13; whereas, Figure 14 shows the FFT plot of these torque profiles under steady-state conditions. The magnitude of the torque ripple for 4p24s, 4p36s, and 4p42s machine models is calculated as 74.18%, 71.22%, and 47.06%. The comparative performance analysis of the investigated machine models employed for the validation of the proposed simplified brushless field-excitation scheme is presented in Table 4.

3.1 | Unbalanced radial force

Brushless WRSMs operate on the principle of the generation of harmonic MMF in the airgap of the machine. This sometimes results in an unbalanced radial force on the rotor of the machine.[20] The unbalanced radial force often has a negative impact on the performance of the machine and results in an unequal stress on its bearings. To evaluate the radial force performance of the studied 4p24s, 4p36s, and 4p42s machine models employed for the validation of the proposed simplified brushless field-excitation scheme FEA is carried out in JMAG-Designer 19.1. The net radial force plot for the investigated models is shown in Figure 15, which indicates that the net radial force has quite satisfactory values for the studied models. The average values of the net radial force are 0.036, 0.278, and 0.149 N for 4p24s, 4p36s, and 4p42s machine models.

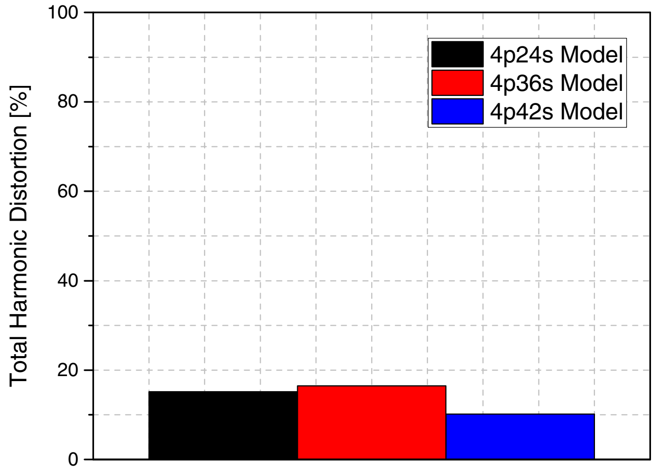

FIGURE 19 Total harmonic distortion of the induced back-electromotive force under the no-load condition for the investigated machine models

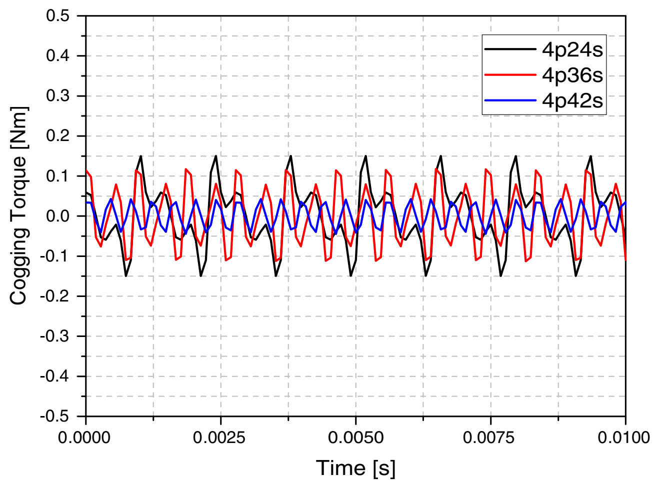

FIGURE 20 Cogging torque for the investigated machine models

TABLE 5 Performance comparison under no-load condition

Attribute	4p24s model	4p36s model	4p42s model
Back-EMF (in V_{rms})	47.00	69.55	76.63
THD of back-EMF (%)	15.2	16.5	10.142
Cogging torque (in Nm)	0.15	0.117	0.042

Abbreviations: EMF, electromotive force; THD, total harmonic distortion.

3.2 | No-load analysis

To investigate the performance of the employed machine models for the validation of the proposed simplified brushless field-excitation scheme under no-load condition, a DC of 1A is used for the rotor field excitation and the machine is operated at 1800 rpm. The magnetic field density distribution plots of the studied machine models under no-load condition are shown in Figure 16; however, Figure 17 illustrates the induced back-EMF of the machine models under such a condition. The magnitude of induced back-EMF for the 4p24s machine model is 47.00 V_{rms}. This magnitude for 4p36s and 4p42s machine models is 69.55 V_{rms} and 76.63 V_{rms}, respectively. The harmonic contents of the induced back-EMF for the studied machine models under no-load condition are shown in Figure 18. Figure 19 illustrates the total harmonic distortion (THD) of the induced back-EMF which shows that the THD for the 4p42s model is around 10.142%, which is the lowest among the investigated machine models. The THD for 4p24s and 4p36s machine models is 15.2% and 16.50%, respectively. The cogging torque of 4p24s, 4p36s, and 4p42s machine models is shown in Figure 20. This figure shows that the magnitude of the cogging torque for 4p24s, 4p36s, and 4p42s machine models is 0.15, 0.117, and 0.042 Nm. Comparative performance analysis of the investigated machine models under the no-load condition is presented in Table 5.

4 | CONCLUSION

A simplified brushless field-excitation scheme for WRSMs was proposed in this paper. Two inverters, which were operated at output frequencies of 60 and 180 Hz, respectively, were used. One of the inverters was supplying three-phase currents to the armature winding at 60 Hz frequency whereas the second inverter was connected to the common point of the star-connected armature winding and was supplying a single-phase current at the frequency of 180 Hz. The composite output of the inverters consisted of the fundamental and third-harmonic. The fundamental was utilized to generate the armature main field, whereas the third-harmonic was employed to induce a 12-pole harmonic current in the rotor harmonic winding. The harmonic current was rectified to excite rotor field winding. FEA was used to verify the proposed simplified brushless scheme and achieve output torque for 4p24s, 4p36s, and 4p42s machine models. From the results, it was concluded that the 4p42s machine model performed well in terms of output torque and torque ripple as compared to 4p24s and 4p36s machine models. In addition, the magnitude of the back-EMF under the no-load condition for the 4p42s machine model was also higher than the 4p24s and 4p36s machine models. Furthermore, the THD of the back-EMF for the 4p42s machine model is lower than the other investigated models as well.

The proposed brushless scheme was based on conventional inverter topologies and did not require any complex algorithm or thyristor switches or machine structure modification, it proved to be simple as compared to the conventional parallel-inverter-controlled and open-winding pattern-based brushless schemes available in the literature without affecting the performance of the machines. Moreover, the proposed scheme involves a single-phase inverter which makes it cost-effective as compared to the brushless WRSM topologies based on dual three-phase inverter configuration.

ACKNOWLEDGMENTS

This work was supported by the Brain Pool (BP) Program funded by the Ministry of Science and ICT through the National Research Foundation of Korea under Grant 2019H1D3A1A01102988 and the Chung-Ang University Research Grants in 2019.

PEER REVIEW

The peer review history for this article is available at https://publons.com/publon/10.1002/2050-7038.12961.

DATA AVAILABILITY STATEMENT

Data sharing not applicable - no new data generated, or the article describes entirely theoretical research

ORCID

Syed Sabir Hussain Bukhari https://orcid.org/0000-0002-3445-4276
Hamza Ahmad https://orcid.org/0000-0001-6125-3827
Jong-Suk Ro https://orcid.org/0000-0003-4429-9393

REFERENCES

1. Yao F, Sun D, Sun L, Lipo TA. Dual Third-Harmonic-Current Excitation Principle of a Brushless Synchronous Machine Based on Double Three-Phase Armature Windings. 2019 22nd International Conference on Electrical Machines and Systems (ICEMS), Harbin, China, 2019:1-4.
2. Bukhari SSH, Sirewal GJ, Ayub M, Ro J. A New Small-Scale Self-Excited Wound Rotor Synchronous Motor Topology. *IEEE Trans Magn*. 2020;57(2):1-5.
3. Basak S, Mondal AK, Chakraborty C. Performance and analysis of a new brushless synchronous generator for DC microgrid application. *IEEE Trans Industry Appl*. 2020;56(3):3137-3148.
4. Zhu S, Hu Y, Liu C, Wang K, Yu J, Zhou Z. Design and analysis of a static excitation part of a brushless wound rotor excitation synchronous machine without an exciter. *IEEE Trans Energy Convers*. 2020;35(3):1182-1195.
5. Ayub M, Bukhari SSH, Jawad G, Kwon BI. Brushless wound field synchronous machine with third-harmonic field excitation using a single inverter. *Electr Eng*. 2019;101:165-173.
6. Di Gioia A et al. Design and demonstration of a wound field synchronous machine for electric vehicle traction with brushless capacitive field excitation. *IEEE Trans Industry Appl*. 2018;54(2):1390-1403.
7. Khan S, Bukhari SSH, Ro J. Design and analysis of a 4-kW two-stack coreless axial flux permanent magnet synchronous machine for low-speed applications. *IEEE Access*. 2019;7:173848-173854.
8. Kano Y. Design optimization of brushless synchronous machines with wound-field excitation for hybrid electric vehicles. 2015 *IEEE Energy Conversion Congress and Exposition (ECCE)* 2015:2769-2775.
9. Stancu C, Ward T, Rahman K, Dawsey R, Savagian P. Separately excited synchronous motor with rotary transformer for hybrid vehicle application. 2014 *IEEE Energy Conversion Congress and Exposition (ECCE)* 2014:1754-1761.
10. Ruuskanen V, Niemela M, Pyrhonen J, Kanerva S, Kaukonen J. Modelling the brushless excitation system for a synchronous machine. *IET Electric Power Appl*. 2009;3(3):231-239.
11. Zhu XY, Cheng M, Zhao WX, Zhang JZ, Hua W. An overview of hybrid excited electric machine capable of field control. *Trans China Electrotechn Soc*. 2008;23(1):30-39.
12. Ayub M, Sirewal GJ, Bukhari SSH, Kwon BI. Brushless wound rotor synchronous machine with third-harmonic field excitation. *Electr Eng*. 2020;102:259-265.
13. Jiao N, Han X, Wei Z, Sun C, Liang P, Liu W. On-line fault diagnosis for rotating rectifier in wound-rotor synchronous starter-generator based on geometric features of current trajectory. *IEEE Trans Industrial Electro*. 2020;68(4):2952-2963.
14. Hussain A, Atiq S, Kwon B-I. Optimal design and experimental verification of wound rotor synchronous machine using subharmonic excitation for brushless operation. *Energies*. 2018;11:554.
15. Ali Q, Hussain A, Baloch N, Kwon BI. Design and optimization of a brushless wound-rotor Vernier machine. *Energies*. 2018;11:317.
16. Choi J, Nam K. Wound synchronous machine Sensorless control based on signal injection into the rotor winding. *Energies*. 2018;11:3278.
17. Ayub M, Atiq S, Sirewal GJ, Kwon B. Fault-tolerant operation of wound field synchronous machine using coil switching. *IEEE Access*. 2019;7:67130-67138.
18. Huang SG, Xia YH, Zhang JM, Liu JG, Zou XQ. The analysis of no-load harmonic electromagnetic field of a harmonic excited synchronous generator. *Electric Mach Control*. 2005;9(1):55-58.
19. Ali Q, Lipo TA, Kwon B-I. Design and analysis of a novel brushless wound rotor synchronous machine. *IEEE Trans. Magn.* 2015;51(11):1-4.
20. Ali Q, Bukhari SSH, Atiq S. Variable-speed, sub-harmonically excited BL-WRSM avoiding unbalanced radial force. *Electr Eng*. 2019;101:251-257.
21. Jawad G, Ali Q, Lipo TA, Kwon BI. Novel brushless wound rotor synchronous machine with zero-sequence third-harmonic field excitation. *IEEE Trans Magn*. 2016;52(7):1-4.
22. Bukhari SSH, Sirewal GJ, Chachar FA, Ro J-S. Dual-inverter-controlled brushless operation of wound rotor synchronous machines based on an open-winding pattern. *Energies*. 2020;13:2205.
23. Sun L, Gao X, Yao F, An Q, Lipo T. A new type of harmonic current excited brushless synchronous machine based on an open winding pattern. *2014 IEEE Energy Conversion Congress and Exposition (ECCE)*, Pittsburgh, PA; 2014:2366-2373.

How to cite this article: Bukhari SSH, Ahmad H, Akhtar F, Ro J-S. Brushless field-excitation method for wound-rotor synchronous machines. *Int Trans Electr Energ Syst*. 2021;e12961. https://doi.org/10.1002/2050-7038.12961